atmosphere

MDPI

Article

Reactivity and Loss Mechanisms of NO_3 and N_2O_5 at a Rural Site on the North China Plain

Dan Wang [1,2], Pinhua Xie [1,3,*], Renzhi Hu [1,*], Zhiyan Li [2], Hao Chen [4] and Huawei Jin [5]

[1] Anhui Institute of Optics and Fine Mechanics, Key Laboratory of Environmental Optics and Technology, Chinese Academy of Sciences, Hefei 230031, China
[2] School of Mathematics and Physics, Anhui University of Technology, Maanshan 243032, China
[3] CAS Center for Excellence in Regional Atmospheric Environment, Institute of Urban Environment, Chinese Academy of Sciences, Xiamen 361000, China
[4] School of Mechanical Engineering, Suzhou University of Science and Technology, Suzhou 215009, China
[5] State Key Laboratory of Mining Response and Disaster Prevention and Control in Deep Coal Mines, Anhui University of Science and Technology, Huainan 232001, China
* Correspondence: phxie@aiofm.ac.cn (P.X.); rzhu@aiofm.ac.cn (R.H.)

Abstract: NO_3, NO_2, O_3, and relevant parameters were measured at a rural site on the North China Plain during June 2014. During the campaign, the average concentrations of NO_3 and N_2O_5 were 4.8 ± 3.3 pptv and 30.5 ± 35.4 pptv, respectively. The average NO_3 production rate was 1.03 ± 0.48 ppbvh^{-1}, and the steady-state lifetimes of NO_3 and N_2O_5 were 26 s and 162 s, respectively, indicating that the NOx chemistry in the rural site during summer was active. The uptake coefficient range of N_2O_5 was 0.023 to 0.118, with an average value of 0.062 ± 0.035. Meanwhile, the fitting for k_{NO_3} was 0.013 ± 0.016 s^{-1}, corresponding to the shorter NO_3 lifetime below 1 min. The results show that the indirect loss pathways caused by the heterogonous uptake of N_2O_5 contributed 64–90% of the overall NO_3 loss, with an average of 81%, suggesting that the N_2O_5 heterogeneous reaction dominated the nocturnal NO_x loss over this region.

Keywords: NO_3; dinitrogen pentoxide; nighttime chemistry; loss mechanisms; heterogonous reaction

check for updates

Citation: Wang, D.; Xie, P.; Hu, R.; Li, Z.; Chen, H.; Jin, H. Reactivity and Loss Mechanisms of NO_3 and N_2O_5 at a Rural Site on the North China Plain. *Atmosphere* **2022**, *13*, 1268. https://doi.org/10.3390/atmos13081268

Academic Editor: Antonietta Ianniello

Received: 30 June 2022
Accepted: 27 July 2022
Published: 10 August 2022

Publisher's Note: MDPI stays neutral with regard to jurisdictional claims in published maps and institutional affiliations.

Copyright: © 2022 by the authors. Licensee MDPI, Basel, Switzerland. This article is an open access article distributed under the terms and conditions of the Creative Commons Attribution (CC BY) license (https://creativecommons.org/licenses/by/4.0/).

1. Introduction

The nitrate radical (NO_3) and dinitrogen pentoxide (N_2O_5) are important reactive nitrogen species with regard to their nighttime chemistry. They play an important role in the nocturnal atmospheric chemistry, which controls the oxidation and removal of various trace gases [1]. O_3 reacts with NO_2 to form NO_3 (Equation (1)), and N_2O_5 is formed by the reaction of NO_3 with NO_2 (Equation (2)), which is in temperature-dependent equilibrium with NO_3 (Equation (3)) [2].

$$NO_2 + O_3 \rightarrow NO_3 + O_2 \quad (1)$$

$$NO_2 + NO_3 + M \rightarrow N_2O_5 + M \quad (2)$$

$$N_2O_5 + M \rightarrow NO_2 + NO_3 + M \quad (3)$$

NO_3 occurs during photolysis during the day and is accumulated only at night (up to several hundred pptv). The rapid reaction with NO is another important sink of NO_3 besides photolysis [3]. NO_3 can oxidize and remove certain volatile organic compounds (VOCs) and sulfides, and its oxidation ability even exceeds that of the daytime OH radical [4]. The terpenes released by natural plants react quickly with the NO_3 radical to form organic nitrate esters, which contributes to the formation of secondary organic aerosol (SOA) [5].

The heterogeneous hydrolysis of N_2O_5 forms soluble nitrate (Equation (4)), and heterogeneously reacts with Cl^- to form $ClNO_2$ and nitrate ($NO_3{}^-$) (Equation (5)). The rate coefficient of the heterogeneous uptake of N_2O_5 is determined by Equation (6) [6]:

$$N_2O_5 + H_2O(l) \rightarrow 2HNO_3 \quad (4)$$

$$N_2O_5 + Cl^-(aq) \rightarrow ClNO_2 + NO_3{}^-(aq) \quad (5)$$

$$k_{N_2O_5} = 0.25\ cS_a\gamma_{N_2O_5} \quad (6)$$

where $k_{N_2O_5}$ is the rate coefficient of the heterogeneous uptake of N_2O_5 and c is the mean molecular velocity of N_2O_5. Here, Sa represents the particle surface area and $\gamma_{N_2O_5}$ is the N_2O_5 uptake coefficient.

High mixing ratios of NO_3 and N_2O_5 have been observed in different environments, such as the Pearl River Delta [7], the North China Plain [8], and Hong Kong [9]. Studies have found that NO_3 and N_2O_5 have the characteristics of strong seasonality and regionality [10–12]. The initial studies on NO_3 mainly focused on its direct and indirect loss pathways [13,14]. Observations and model simulations have been used to study the heterogeneous N_2O_5 uptake, which is an important pathway of NO_X loss [15]. The N_2O_5 uptake coefficients in different environmental conditions were obtained to evaluate NO_X loss [16] and the contribution of nocturnal NO_3 to the formation of secondary organic aerosol has been studied [17]. In recent years, to investigate the nocturnal chemical processes of NOx, some field observations have been carried out in China. However, comprehensive field studies of N_2O_5 and NO_3 simultaneously have been relatively rare at rural sites on the North China Plain. On account of the importance of NO_3 and N_2O_5 in nocturnal atmospheric chemistry, it is of great interest to investigate the nocturnal chemical processes of NOx in the North China Plain.

In this study, self-developed cavity ring down spectroscopy (CRDS) was applied for the 2014 CAREBEIJING-NCP field experimental observation in summer (Wangdu, China). We report on observations of NO_3, N_2O_5, and relevant species. The factors influencing the production rate and lifetimes of NO_3 and N_2O_5 were deeply analyzed. In addition, heterogeneous N_2O_5 uptake coefficient was estimated and the loss mechanisms of NO_3 and N_2O_5 were further studied over this region during the summer time.

2. Method

2.1. Site Description

Cavity ring-down spectroscopy (CRDS) was applied for the Campaigns of Air Pollution Research in Megacity Beijing and North China Plain (CAREBEIJING-NCP) in Wangdu County, Hebei Province (38.665° N, 115.204° E) from 10 June to 6 July 2014, which was 170 km southwest of Beijing (Figure 1). The site was surrounded by crops, near the S032 and G4 expressways. The CRDS instrument was located on the fourth floor of the building, approximately 10 m above the ground (sample tubes of 1.1 m). As the measurement site was close to the national road, the NO_3 radical measurement results were susceptible to interference from vehicle emissions. During the observation period, northeasterly winds and easterly winds (from the direction of the G4 national highway) prevailed and the wind speed was relatively high, with a maximum wind speed of 26.5 m/s and an average wind speed of about 4.2 m/s (Figure 2).

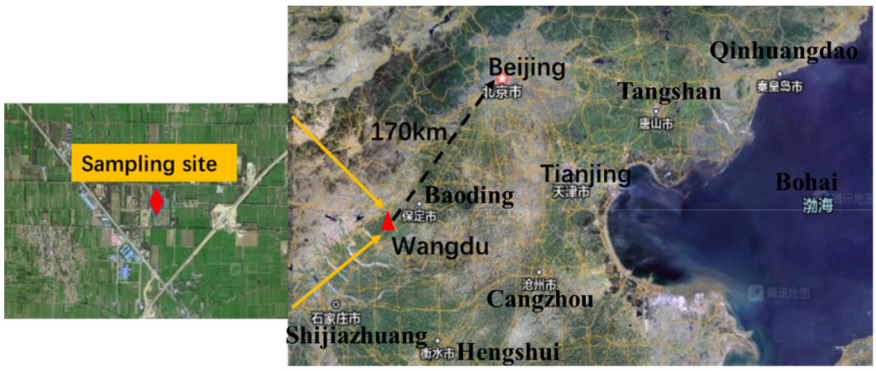


Figure 1. Field measurement site in Wangdu, Hebei Province.

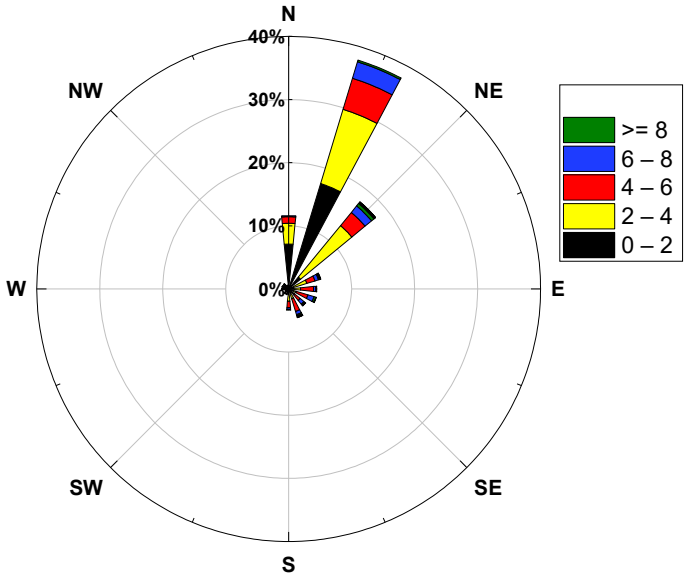


Figure 2. Wind speed and wind direction.

2.2. Instruments

The principles of the CRDS instrument have been described previously [18,19]. The same CRDS instrument was applied in Wangdu, Hebei Province. The light from the laser diode with a center wavelength of 661.85 nm was coupled to an optical cavity. The cavity was formed using a pair of high-reflectivity mirrors ($R \geq 99.9985\%$). The light transmitted through the back mirrors was detected by a photomultiplier tube and then the signals were digitized using an oscilloscope card controlled by the LabVIEW program. The 1500 decay profiles were co-added to achieve a higher signal/noise ratio. Then, the decay trace was fitted by the Levenberg–Marquardt algorithm to obtain the ring-down time. The CRDS instrument was located approximately 10 m above the ground. The sample tubes of the CRDS instrument equaled 1.1 m and the sampling flow was 5 standard liters per minute. The detection limit of the NO_3 radical determined by Allan variance was approximately 1.6 pptv (1σ, 10 s). The uncertainty for NO_3 was about $\pm 8\%$.

The relevant trace gases were measured simultaneously during the field observations. N_2O_5 was observed using a chemical ionization mass spectrometer (THS Instruments, Atlanta), and the detection limit was 7 pptv (3σ, 1 min). NO and NO_2 were obtained using a chemiluminescence analyzer (Thermo Fisher 42i, Waltham, MA, USA). O_3 was observed using an ultraviolet (UV) absorption analyzer (0.5 ppbv, 1 min). The meteorological parameters, including the wind direction, wind speed, relative humidity (RH), and temperature, were observed using an ultrasonic anemometer and a weather station, which were located

10 m above the ground. The aerosol surface (Sa) was obtained using a scanning mobility particle sizer (SMPS) and aerodynamic particle sizer (TSI-type APS model 3321).

3. Results and Discussion

3.1. Overview of Measurements

During the measurement period, the temperature and RH showed an obvious diurnal variation trend, and the variation trend was obviously opposite. When the atmospheric temperature was low at night, the RH reached the maximum. During the day, the temperatures peak around noon. During the observation period, the RH levels varied from 14% to 98%, and the average humidity was 62.7%. At the same time, the temperatures were higher, with an average temperature of 299.2 K, indicating that the whole campaign was conducted in high-temperature and -humidity environments.

The time series of NO_3 concentrations observed using the CRDS instrument and the relevant parameters is shown in Figure 3. During the observation period from June 10th to 6 July, the NO_3 nocturnal concentration varied from 0 to 25 pptv, and the average nocturnal concentration was about 4.8 $\pm$ 3.3 pptv. The highest NO_3 nocturnal concentration reached 25 pptv on 15 June and 27 June. There were prevailing northeasterly winds and easterly winds during the measurement period, and the measurement site was close to the national road and easily affected by local sources of vehicle emissions, which may have contributed to the relatively low NO_3 concentrations. The O_3 concentrations showed obvious periodicity, with peak concentration occurring around 16:00, with a maximum of 140 ppbv, which decreased to the detection limit after midnight. The O_3 concentrations were relatively high during the whole observation period, with an average concentration of 54 ppbv, which implied intense photochemical reactions during the observations. The NO_2 concentrations showed an inverse correlation with O_3, with an average value of 9.6 ppbv. During the measurement period, due to the influence of automobile emission sources, The NO concentrations were relatively high and several instantaneous peaks appeared during the observation period.

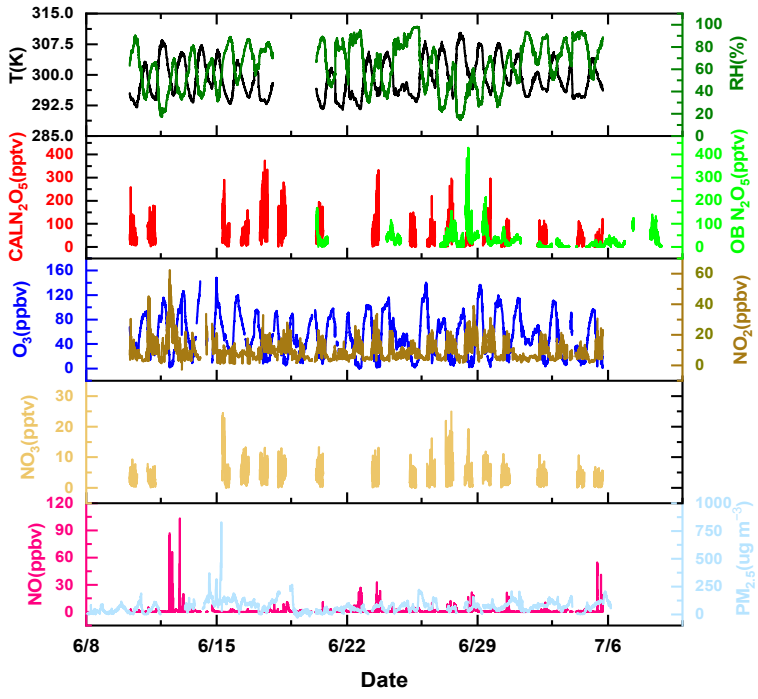


Figure 3. Time series of N_2O_5, NO_3, and related trace gases. OB N_2O_5 is the mixing ratio of N_2O_5 observed by CIMS, and CAL N_2O_5 is the mixing ratio of N_2O_5 calculated by NO_3 and NO_2.

Here, the mixing ratio of N_2O_5 can be calculated using Equation (7). During the whole nocturnal observation period from June 10th to July 6th, the calculated N_2O_5 concentrations were relatively high, with a maximum of 374 pptv, which mainly attributed to the high mixing ratio of NO_3 and NO_2. The mixing ratio of observed N_2O_5 was measured via CIMS, which showed a high concentration during the period of 27 June to 29 June, with a maximum concentration of 429 pptv. The average concentration of observed N_2O_5 was 30.5 ± 35.4 pptv.

$$[N_2O_5] = \text{Kep}\ [NO_2][NO_3] \quad (7)$$

$$P(NO_3) = k_{NO_2+O_3}\ [NO_2][O_3] \quad (8)$$

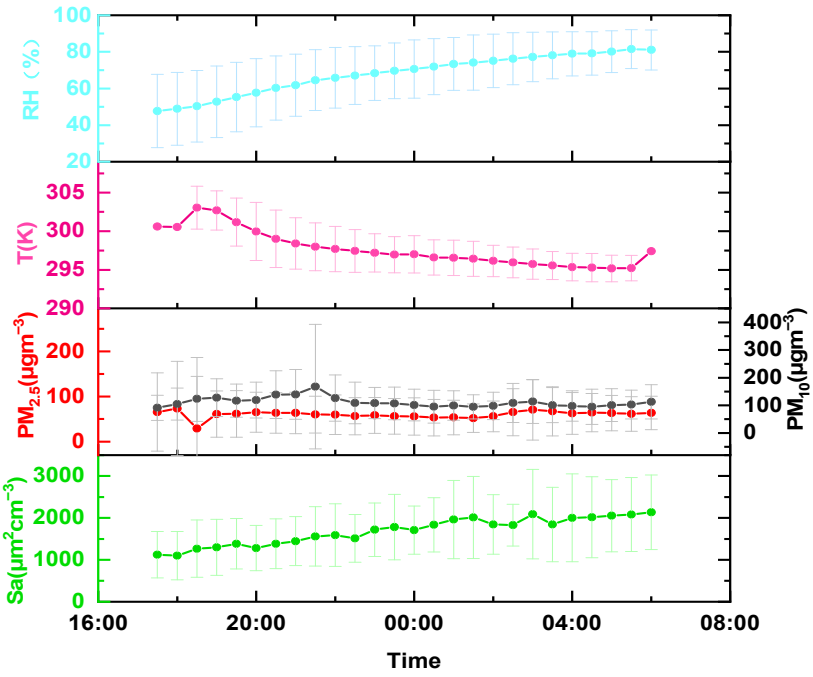
where $k_{NO_2+O_3}$ is the rate constant for the reaction of NO_2 with O_3 and Kep is the equilibrium constant dependent on the temperature.

3.2. NO_3 Production Rate and N_2O_5

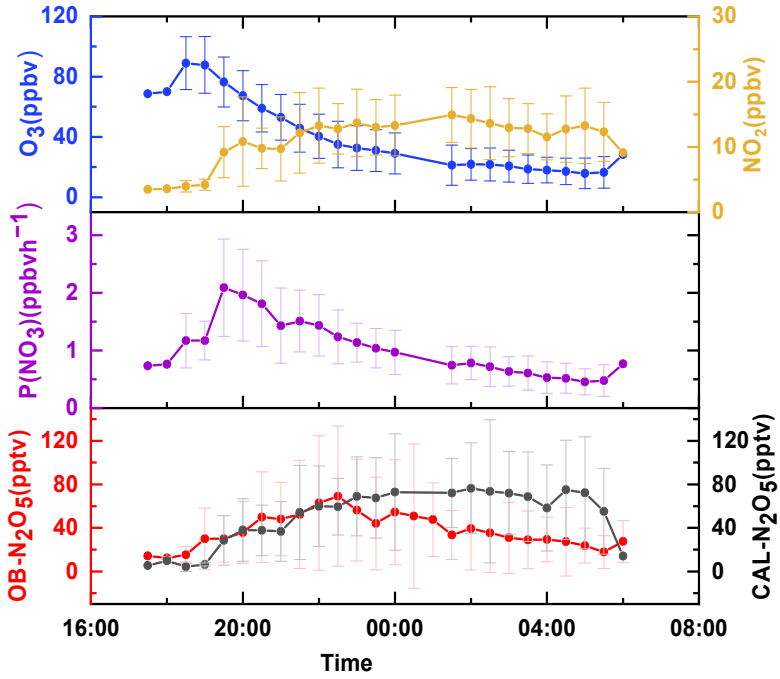
Figure 4a shows the nocturnal profiles for the temperature, humidity, $PM_{2.5}$, PM_{10}, and Sa. During the nighttime period, the average temperature was 298 K and the maximum temperature appeared at 18:30. The nocturnal humidity increased gradually, with an average value of 68%. The $PM_{2.5}$ concentration was lower, below 50 μgm^{-3}. Sa also presented a steadily rising trend, with an average value of 1687 $\mu m^2 cm^{-3}$.

The NO_3 production rate ($P(NO_3)$) was calculated using Equation (8) [20]. The mean nocturnal variations of NO_2, O_3, N_2O_5, and $P(NO_3)$ are shown in Figure 4b. During the nighttime period, the average concentrations of O_3 and NO_2 were 41.1 ± 24.1 ppbv and 10.9 ± 3.6 ppbv, respectively. The NO_2 and O_3 were highly inversely correlated. The O_3 concentrations decreased after sunset, while the NO_2 concentrations slightly increased. The $P(NO_3)$ showed a similar trend with O_3, and was mainly affected by the O_3 variation. The peak of $P(NO_3)$ appeared at 19:00–20:00 (an hour after the ozone peak), reaching 2.09 $ppbvh^{-1}$. The value for $P(NO_3)$ was 1.03 ± 0.48 $ppbvh^{-1}$, which was slightly lower than that observed on a tower in Seoul (1.3 $ppbvh^{-1}$) [21] and in Beijing (1.2 $ppbvh^{-1}$) [22]. The average nighttime $P(NO_3)$ value was slightly larger than that at a suburban site in Taizhou (1.01 $ppbvh^{-1}$) [17]. The comparison showed the significant oxidation capacity of NO_3 in Wangdu County.

The linear correlation coefficient between $P(NO_3)$ and O_3 is plotted in Figure 5a. The average temperature was 297.7 K during the nighttime period, and the high temperature promoted NO_3 formation. The higher the temperature, the higher the $P(NO_3)$, as shown in Figure 5a, which illustrated that the temperature was one of the main factors controlling the NO_3 formation. The other two factors, NO_2 and O_3, also determined the $P(NO_3)$. The linear correlation coefficient between $P(NO_3)$ and O_3 was 0.68, which was higher than for NO_2 (R = 0.06). The N_2O_5 concentration also showed a clear positive dependence on O_3 (Figure 5b). This result may imply that the $P(NO_3)$ and N_2O_5 concentrations mainly varied with the O_3 concentrations, which could partly explain why O_3 varied more rapidly than NO_2 during the observation period.

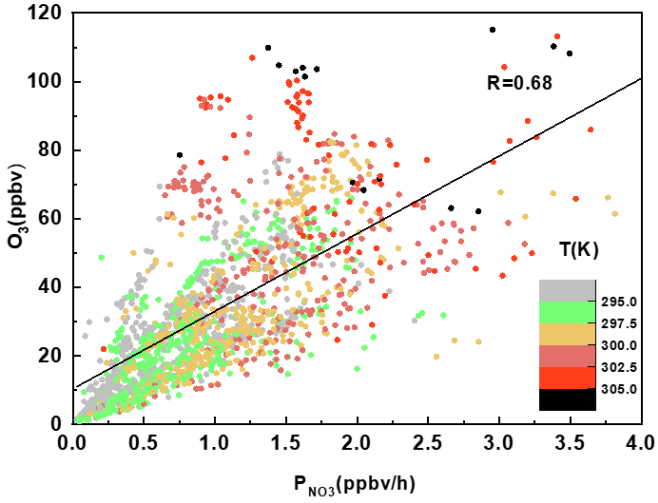


(**a**)

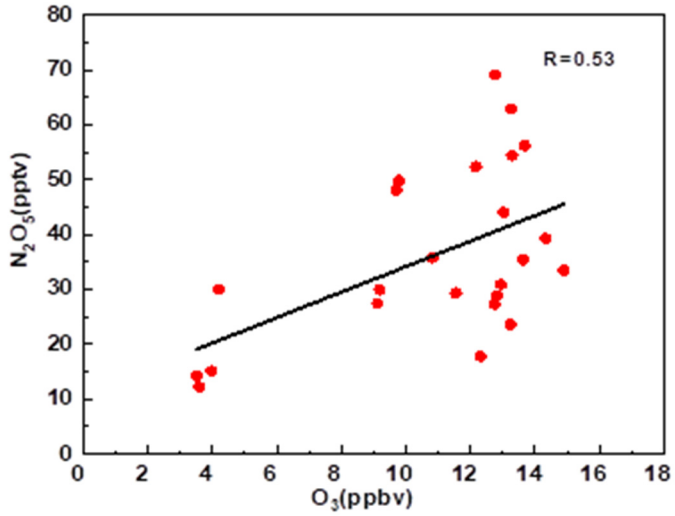


(**b**)

Figure 4. (**a**) Mean nocturnal profiles of temperature, humidity, $PM_{2.5}$, PM_{10}, and Sa in this campaign. (**b**) Mean nocturnal profiles of NO_2, O_3, N_2O_5, and $P(NO_3)$ during the measurement period; the error bar is the standard deviation. OB N_2O_5 is the mixing ratio of N_2O_5 observed by CIMS, and CAL N_2O_5 is the mixing ratio of N_2O_5 calculated by NO_3 and NO_2.



(**a**)



(**b**)

Figure 5. (**a**) The dependence of $P(NO_3)$ on the O_3 concentration. The black line shows linear fitting. (**b**) The dependence of N_2O_5 on the O_3 concentration. The black line shows linear fitting.

During the measurement period, the mean nocturnal variations of the calculated N_2O_5 and observed N_2O_5 showed the same trend and their concentrations were basically consistent before midnight, with the large discrepancy shown after midnight. After midnight, the humidity was above 70 percent, which accelerated the heterogeneous hydrolysis of N_2O_5. The discrepancy between the calculated N_2O_5 and observed N_2O_5 was mainly ascribed to the heterogonous uptake of N_2O_5. The observed N_2O_5 concentration gradually increased after sunset, peaking near 22:30. After 00:00, $P(NO_3)$ and N_2O_5 decreased simultaneously, suggesting that the low concentration of N_2O_5 was partly attributed to the lack of NO_3 formation.

3.3. Steady-State Lifetimes of NO_3 and N_2O_5

The steady-state lifetime was applied extensively when evaluating N_2O_5 and NO_3, and can be represented as in Equations (9) and (10) [23]:

$$\tau(NO_3) = \frac{[NO_3]}{k_{NO_2+O_3}[NO_2][O_3]} \quad (9)$$

$$\tau(N_2O_5) = \frac{[N_2O_5]}{k_{NO_2+O_3}[NO_2][O_3]} \quad (10)$$

During the whole campaign, the nocturnal N_2O_5 lifetime varied from 4 s to 13 min, with an average value of 162 s, while the average NO_3 lifetime was 26 s (Figure 6). Table 1 shows the observed N_2O_5 concentration and $P(NO_3)$ and $\tau(N_2O_5)$ values in Wangdu and other observation sites. The lifetime of N_2O_5 in this study was slightly lower than the obtained N_2O_5 lifetime in Beijing (310 s, average) [22], but was much shorter than that in Hong Kong (0.2–3 h) [9] and that in Seoul, Korea (0.5 h, average) [21]. The shorter lifetime in Wangdu indicated that N_2O_5 and NO_3 were highly reactive and rapidly exhausted.

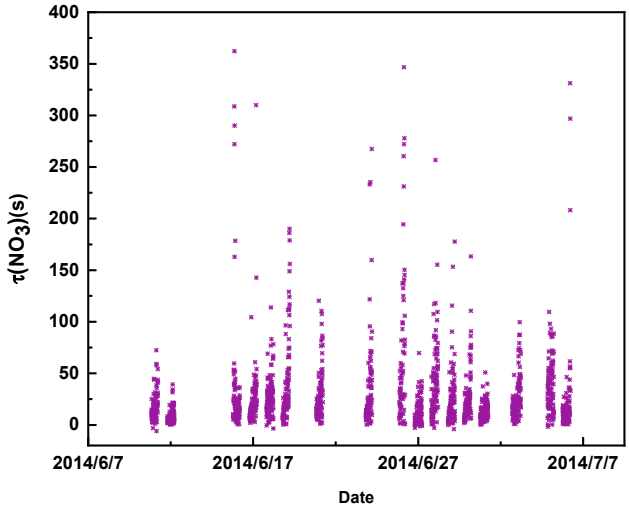


Figure 6. Time series for the NO_3 lifetime in Wangdu County, Hebei Province, from 10 June to 6 July.

Table 1. The N_2O_5 concentration and $P(NO_3)$ and $\tau(N_2O_5)$ values in Wangdu and other observation sites.

Location	Environment	N_2O_5 (pptv)	$P(NO_3)$ (ppbvh^{-1})	$\tau(N_2O_5)$	Reference
Beijing, China	Urban	<1100	1.2 ± 0.9	310 ± 240 s	[22]
Seoul, Korea	Urban, Tower	<5000	1.3	0.5 h	[21]
Hong Kong, China	Rural mountaintop	<8000	0.32	0.2–3 h	[9]
Taizhou, China	Suburban	<700	1.2 ± 0.4	55 ± 68 s	[24]
Wangdu, China	Rural	<500	1.03 ± 0.48	162 s	This study

The influencing factors of the N_2O_5 lifetime were analyzed using the related parameters. When the RH exceeded 55%, the N_2O_5 lifetime showed a clear negative dependence on RH (Figure 7). The high RH effectively reduced the N_2O_5 lifetime, indicating that the heterogeneous N_2O_5 process played a large role as a sink. Figure 7b shows the correlation between the N_2O_5 lifetime and Sa. Here, the $\tau(N_2O_5)$ rapidly decreased from 4 min to 1 min as the Sa increased up to 1250 μm^2 cm^{-3}, but was approximately constant when the Sa increased from 1750 μm^2 cm^{-3} to 3750 μm^2 cm^{-3}. The variation trend for the N_2O_5 lifetime with Sa indicated that the N_2O_5 uptake rates increased at higher Sa values. The N_2O_5 uptake was an important part of the N_2O_5 loss, which was promoted by the high RH and Sa.

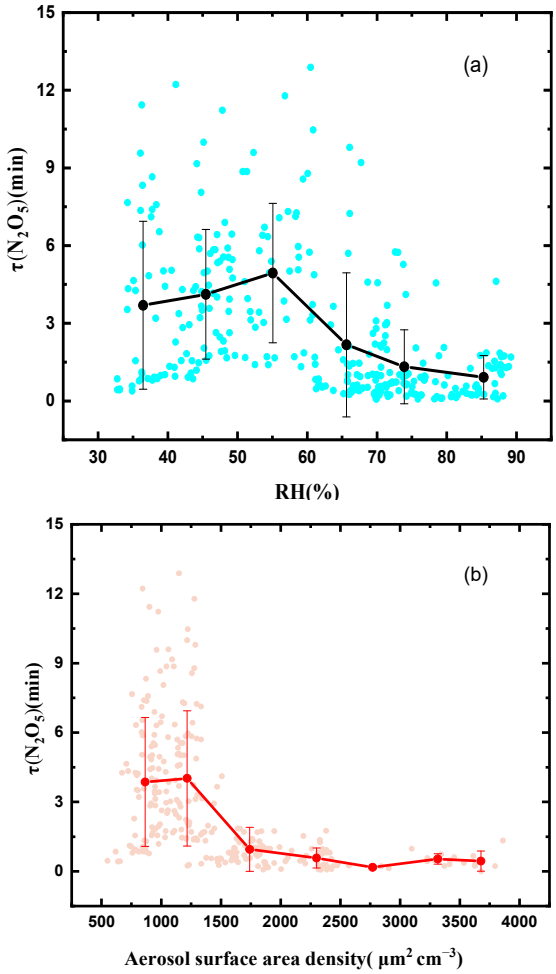


Figure 7. Scatter plots of the N_2O_5 lifetime versus RH (**a**) and scatter plots of the N_2O_5 lifetime versus Sa (**b**).

3.4. NO_3 and N_2O_5 Loss Pathways

The loss of NO_3 was generally divided into two kinds, direct loss pathways caused by the reaction with the VOCs and NO and indirect loss pathways caused by N_2O_5 heterogeneous hydrolysis. To delve into the loss rates, the N_2O_5 uptake coefficient was estimated using steady-state methods (Equation (13)) [6]. The linear fits showed the N_2O_5 uptake coefficient, $\gamma_{N_2O_5}$, as the slope and the first-order loss rate coefficient for NO_3, k_{NO_3}, as the intercept.

$$\tau(NO_3)^{-1} = k_{NO_3} + K_{eq}[NO_2]k_{N_2O_5} \quad (11)$$

$$\tau(N_2O_5)^{-1} = k_{N_2O_5} + \frac{k_{NO_3}}{K_{eq}[NO_2]} \quad (12)$$

$$\tau(N_2O_5)^{-1}K_{eq}[NO_2] = \frac{1}{4}cS_a\gamma_{N_2O_5}K_{eq}[NO_2] + k_{NO_3} \quad (13)$$

In this study, which lasted only five nights, we obtained valid fitting results. The uptake coefficient range of N_2O_5 was 0.023 to 0.118, and the average uptake coefficient was 0.062 ± 0.035 (Figure 8). The high $\gamma_{N_2O_5}$ was associated with the RH and Sa. Compared with the other fields, the obtained N_2O_5 uptake coefficient in this study was larger than those observed in Hong Kong (0.014 ± 0.007) [9], New England (0.001–0.017) [20], Calgary (0.02) [25], and London (0.01–0.03) [26]. However, the value of $\gamma_{N_2O_5}$ was similar to that in Taizhou (0.027–0.107) [24].

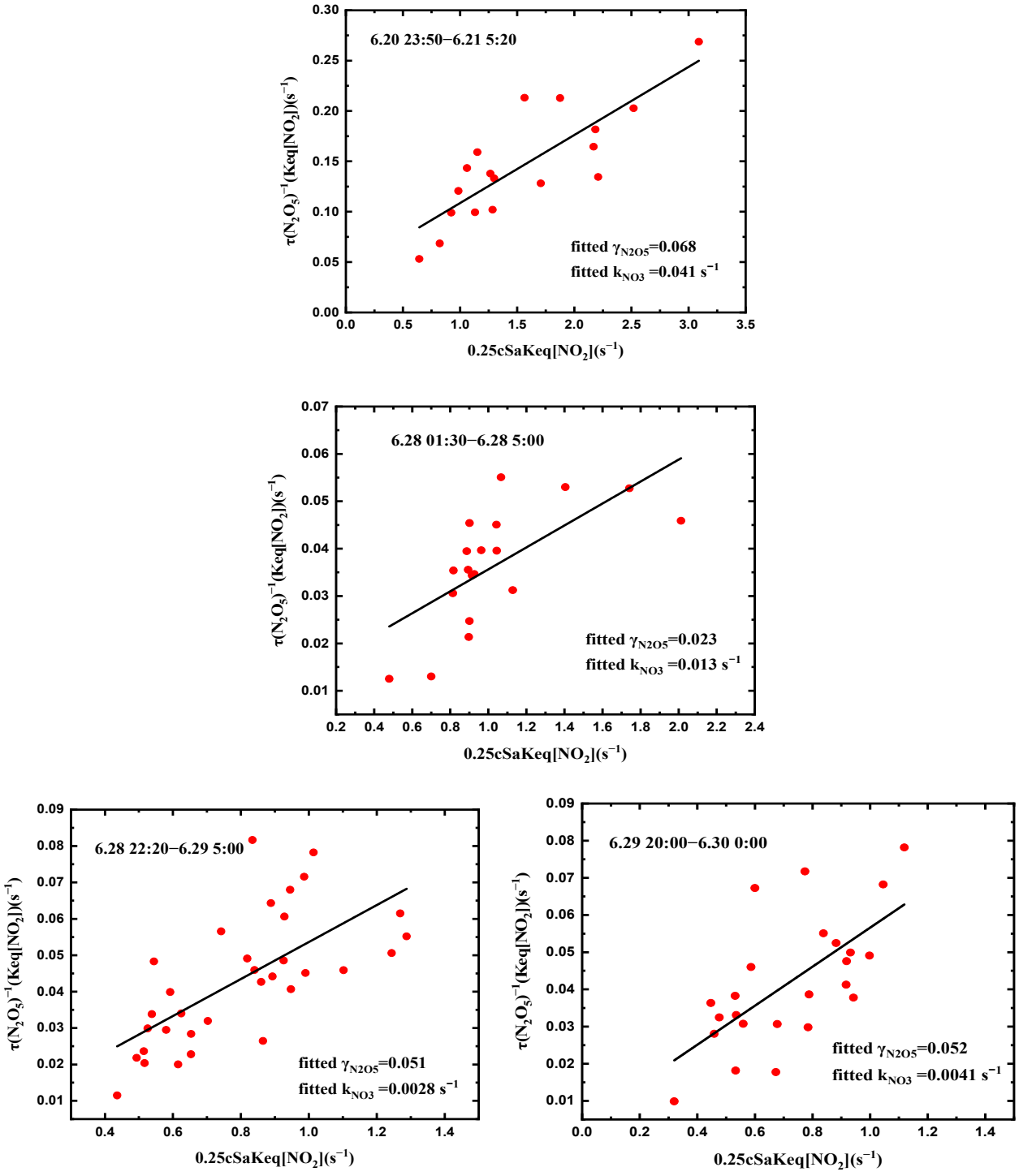


Figure 8. *Cont.*

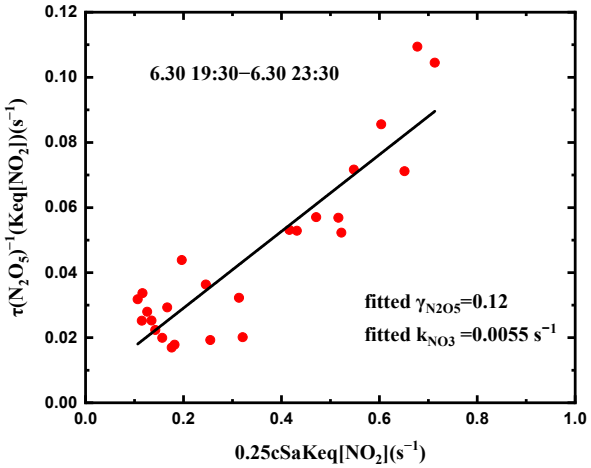


Figure 8. The N_2O_5 uptake coefficient is the slope of the linear fits of $\tau(N_2O_5)^{-1}K_{eq}[NO_2]$ versus $0.25cS_aK_{eq}[NO_2]$; k_{NO_3} is the intercept of the linear fits.

The k_{NO_3} values varied from 0.0028 s^{-1} to 0.041 s^{-1}, and the average was 0.013 ± 0.016 s^{-1}, corresponding to the shorter NO_3 lifetime below 1 min (Table 2). The high k_{NO_3} indicated that the reactions of NO_3 with NO and the VOCs represented important sinks. The NO_3 removal process caused by the reactions with the VOCs and NO accounted for about 10–36% of the total during the five nighttime cases. The rate coefficient of the heterogeneous uptake of N_2O_5 ($k_{N_2O_5}$) can be calculated using Equation (6). The values of $k_{N_2O_5}$ varied from 0.0016 s^{-1} to 0.077 s^{-1}, with an average value of 0.046 ± 0.029 s^{-1} during the five nighttime cases. The indirect loss pathways caused by the heterogonous uptake of N_2O_5 were estimated, which contributed 64–90% of the overall NO_3 loss (average of 81%), suggesting the dominance of the heterogeneous reaction of N_2O_5 in nocturnal NO_3 loss. Compared with the studies in South China, the loss of NOx was dominated by the VOCs followed by N_2O_5 uptake in Tai'Zhou in polluted Southern China [17].

Table 2. The N_2O_5 uptake coefficient, $k(_{NO_3})$, and $k_{N_2O_5}$.

Date	Sa ($\mu m^2/cm^3$)	$\gamma_{N_2O_5}$	$K_{N_2O_5}$ (s^{-1})	K_{NO_3} (s^{-1})
20–21 June	1876	0.068	0.0077	0.041
27–28 June	1185	0.023	0.0016	0.013
27–28 June	926	0.051	0.0027	0.0028
29–30 June	1090	0.052	0.0034	0.0041
30 June–1 July	1077	0.118	0.0077	0.0055

4. Conclusions

During the measurement period, the maximum concentrations of nocturnal NO_3 and N_2O_5 were 25 pptv and 429 pptv. The $P(NO_3)$ varied mainly with the ambient O_3 concentrations. The observed N_2O_5 concentration gradually increased after sunset, mostly peaking near 22:30. The nocturnal average lifetimes of NO_3 and N_2O_5 were 26 s and 162 s, which were 3-fold smaller than that reported in Beijing, The shorter lifetime in Wangdu indicated that the N_2O_5 and NO_3 were highly reactive and rapidly exhausted over this region in the North China Plain. The estimated heterogeneous N_2O_5 uptake coefficient range was 0.023 to 0.118 during the five nighttime cases. The indirect loss by the heterogonous N_2O_5 uptake was estimated, which contributed 64–90% of the overall NO_3 loss. The N_2O_5 lifetime had a clear negative dependence on the RH and Sa. The high RH and high Sa may have promoted the heterogonous N_2O_5 uptake during the campaign.

Without the quantification of the contribution of the VOCs to NOx loss during the campaign, the above analysis based on the N_2O_5 uptake coefficient may have some uncertainties. The results in this work demonstrate the importance of the heterogeneous

chemistry in nocturnal NO_3 and N_2O_5 removal in rural sites on the North China Plain. Meanwhile, it may be applicable to the N_2O_5 uptake processes in similar regions with high NOx, high RH, and high Sa.

Author Contributions: Supervision, R.H. and P.X.; Methodology and writing—original draft preparation, D.W.; investigation, Z.L., H.C. and H.J. All authors have read and agreed to the published version of the manuscript.

Funding: This research was funded by the National Natural Science Foundation of China (Grant No. 41905130), the Natural Science Foundation of Anhui Province of China (Grant Nos. 1908085QD159, 2008085QD182), the Major Project of Natural Science Research in Universities of Anhui Province (KJ2021ZD0052), and the China Postdoctoral Science Foundation (No. 2020M671383).

Institutional Review Board Statement: Not applicable.

Informed Consent Statement: Not applicable.

Data Availability Statement: Not applicable.

Acknowledgments: This work was supported by the National Natural Science Foundation of China (Grant No. 41905130), the Natural Science Foundation of Anhui Province of China (Grant Nos. 1908085QD159, 2008085QD182), the Major Project of Natural Science Research in Universities of Anhui Province (KJ2021ZD0052), and the China Postdoctoral Science Foundation (No. 2020M671383). We give special thanks to Yee Jun and Tao Wang of the Hong Kong Polytechnic University for their support of this study.

Conflicts of Interest: The authors declare no conflict of interest.

References

1. Geyer, A.; Ackermann, R.; Dubois, R.; Lohrmann, B.; Muller, T.; Platt, U. Long-term observation of nitrate radicals in the continental boundary layer near Berlin. *Atmos. Environ.* **2001**, *35*, 3619–3631. [CrossRef]
2. Benton, A.K.; Langridge, J.M.; Ball, S.M.; Bloss, W.J.; Dall'Osto, M.; Nemitz, E.; Harrison, R.M.; Jones, R.L. Night-time chemistry above London: Measurements of NO_3 and N_2O_5 from the BT Tower. *Atmos. Chem. Phys.* **2010**, *10*, 9781–9795. [CrossRef]
3. Volkamer, R.; Sheehy, P.; Molina, L.T.; Molina, M.J. Oxidative capacity of the Mexico city atmosphere—Part 1: A radical source perspective. *Atmos. Chem. Phys.* **2010**, *10*, 6969–6991. [CrossRef]
4. Wayne, R.P.; Barnes, I.; Biggs, P.; Burrows, J.P.; Canosamas, C.E.; Hjorth, J.; Lebras, G.; Moortgat, G.K.; Perner, D.; Poulet, G.; et al. The nitrate radical—Physics, chemistry, and the atmosphere. *Atmos. Environ. Part A Gen. Top.* **1991**, *25*, 1–203. [CrossRef]
5. Ng, N.L.; Brown, S.S.; Archibald, A.T.; Atlas, E.; Cohen, R.C.; Crowley, J.N.; Day, D.A.; Donahue, N.M.; Fry, J.L.; Fuchs, H.; et al. Nitrate radicals and biogenic volatile organic compounds: Oxidation, mechanisms, and organic aerosol. *Atmos. Chem. Phys.* **2017**, *17*, 2103–2162. [CrossRef] [PubMed]
6. Chang, W.L.; Bhave, P.V.; Brown, S.S.; Riemer, N.; Stutz, J.; Dabdub, D. Heterogeneous atmospheric chemistry, ambient measurements, and model calculations of N_2O_5: A review. *Aerosol Sci. Technol.* **2011**, *45*, 665–695. [CrossRef]
7. Yun, H.; Wang, W.; Wang, T.; Xia, M.; Yu, C.; Wang, Z.; Poon, S.C.N.; Yue, D.; Zhou, Y. Nitrate formation from heterogeneous uptake of dinitrogen pentoxide during a severe winter haze in southern China. *Atmos. Chem. Phys.* **2018**, *18*, 17515–17527. [CrossRef]
8. Wang, X.; Wang, H.; Xue, L.; Wang, T.; Wang, L.; Gu, R.; Wang, W.; Tham, Y.J.; Wang, Z.; Yang, L.; et al. Observations of N_2O_5 and $ClNO_2$ at a polluted urban surface site in North China: High N_2O_5 uptake coefficients and low $ClNO_2$ product yields. *Atmos. Environ.* **2017**, *156*, 125–134. [CrossRef]
9. Brown, S.S.; Dube, W.P.; Tham, Y.J.; Zha, Q.Z.; Xue, L.K.; Poon, S.; Wang, Z.; Blake, D.R.; Tsui, W.; Parrish, D.D.; et al. Night-time chemistry at a high altitude site above Hong Kong. *J. Geophys. Res. Atmos.* **2016**, *121*, 2457–2475. [CrossRef]
10. Zhou, W.; Zhao, J.; Ouyang, B.; Mehra, A.; Xu, W.; Wang, Y.; Bannan, T.J.; Worrall, S.D.; Priestley, M.; Bacak, A.; et al. Production of N_2O_5 and $ClNO_2$ in summer in urban Beijing, China. *Atmos. Chem. Phys.* **2018**, *18*, 11581–11597. [CrossRef]
11. Li, Z.; Wang, D.; Xie, P.; Hu, R.; Chen, H.; Lin, C. Nighttime N_2O_5 chemistry in an urban site of Beijing in winter based on the measurements by cavity ring-down spectroscopy. *Air Qual. Atmos. Health* **2022**, *15*, 867–876. [CrossRef]
12. Yun, H.; Wang, T.; Wang, W.; Tham, Y.J.; Li, Q.; Wang, Z.; Poon, S.C. Nighttime NOx loss and $ClNO_2$ formation in the residual layer of a polluted region: Insights from field measurements and an iterative box model. *Sci. Total Environ.* **2018**, *622*, 727–734. [CrossRef] [PubMed]
13. Li, S.; Liu, W.; Xie, P.; Qin, M.; Yang, Y. Observation of Nitrate Radical in the Nocturnal Boundary Layer During a Summer Field Campaign in Pearl River Delta, China. *Terr. Atmos. Ocean. Sci.* **2012**, *23*, 39–48. [CrossRef]
14. Wang, D.; Hu, R.Z.; Xie, P.H.; Qin, M.; Xing, X.B. Nocturnal Atmospheric NO_3 Radical Monitoring and Analysis in Beijing with Cavity Ring Down System. *Spectrosc. Spect. Anal.* **2016**, *36*, 3097–3102.

15. Wang, H.; Lu, K.; Tan, Z.; Sun, K.; Li, X.; Hu, M.; Shao, M.; Zeng, L.; Zhu, T.; Zhang, Y. Model simulation of NO_3, N_2O_5 and $ClNO_2$ at a rural site in Beijing during CAREBeijing-2006. *Atmos. Res.* **2017**, *196*, 97–107. [CrossRef]
16. Wang, Z.; Wang, W.; Tham, Y.J.; Li, Q.; Wang, H.; Wen, L.; Wang, X.; Wang, T. Fast heterogeneous N_2O_5 uptake and $ClNO_2$ production in power plant and industrial plumes observed in the nocturnal residual layer over the North China Plain. *Atmos. Chem. Phys.* **2017**, *17*, 12361–12378. [CrossRef]
17. Wang, H.; Chen, X.; Lu, K.; Hu, R.; Li, Z.; Wang, H.; Ma, X.; Yang, X.; Chen, S.; Dong, H.; et al. NO_3 and N_2O_5 chemistry at a suburban site during the EXPLORE-YRD campaign in 2018. *Atmos. Environ.* **2020**, *224*, 117180. [CrossRef]
18. Wang, D.; Hu, R.; Xie, P.; Liu, J.; Liu, W.; Qin, M.; Ling, L.; Zeng, Y.; Chen, H.; Xing, X.; et al. Diode laser cavity ring-down spectroscopy for in situ measurement of NO_3 radical in ambient air. *J. Quant. Spectrosc. Radiat. Transf.* **2015**, *166*, 23–29. [CrossRef]
19. Wang, D.; Hu, R.; Xie, P.; Li, Z. A novel calibration method for atmospheric NO_3 radical via high reflectivity cavity. *Meas. Sci. Technol.* **2020**, *31*, 085801. [CrossRef]
20. Brown, S.S.; Ryerson, T.B.; Wollny, A.G.; Brock, C.A.; Peltier, R.; Sullivan, A.P.; Weber, R.J.; Dubé, W.P.; Trainer, M.; Meagher, J.F.; et al. Variability in nocturnal nitrogen oxide processing and its role in regional air quality. *Science* **2006**, *311*, 67–70. [CrossRef]
21. Brown, S.S.; An, H.; Lee, M.; Park, J.-H.; Lee, S.-D.; Fibiger, D.L.; McDuffie, E.E.; Dubé, W.P.; Wagner, N.L.; Min, K.-E. Cavity en-hanced spectroscopy for measurement of nitrogen oxides in the Anthropocene: Results from the Seoul tower during MAPS 2015. *Faraday Discuss.* **2017**, *200*, 529–557. [CrossRef] [PubMed]
22. Wang, H.; Lu, K.; Guo, S.; Wu, Z.; Shang, D.; Tan, Z.; Wang, Y.; Le Breton, M.; Lou, S.; Tang, M.; et al. Efficient N_2O_5 uptake and NO_3 oxidation in the outflow of urban Beijing. *Atmos. Chem. Phys.* **2018**, *18*, 9705–9721. [CrossRef]
23. Platt, U.; Perner, D.; Winer, A.M.; Harris, G.W.; Pitts, J.N. Detection of NO_3 in the polluted troposphere by differential optical-absorption. *Geophys. Res. Lett.* **1980**, *7*, 89–92. [CrossRef]
24. Li, Z.; Xie, P.; Hu, R.; Wang, R.; Jin, H.; Chen, H.; Lin, C.; Liu, W. Observations of N_2O_5 and NO_3 at a suburban environment in Yangtze river delta in China: Estimating heterogeneous N_2O_5 uptake coefficients. *J. Environ. Sci.* **2020**, *95*, 248–255. [CrossRef]
25. Mielke, L.H.; Furgeson, A.; Osthoff, H.D. Observation of $ClNO_2$ in a mid-continental urban environment. *Environ. Sci. Technol.* **2011**, *45*, 8889–8896. [CrossRef]
26. Morgan, W.T.; Ouyang, B.; Allan, J.D.; Aruffo, E.; Di Carlo, P.; Kennedy, O.J.; Lowe, D.; Flynn, M.J.; Rosenberg, P.D.; Williams, P.I.; et al. In-fluence of aerosol chemical composition on N_2O_5 uptake: Air-borne regional measurements in northwest-ern Europe. *Atmos. Chem. Phys.* **2015**, *15*, 973–990. [CrossRef]